lag analysis, can be applied to explain this transverse cracking in cross-ply laminates, with some changes to account for wave propagation effects; however, the development of this approach requires further work.

Acknowledgement

The authors wish to acknowledge the U.S. Army Research Office, Durham, NC, for their support of this research programme under Grant No. DAAG29-79-G-0007.

References

1. N. CRISTESCU, L. E. MALVERN and R. L. SIERAKOWSKI, "Foreign Object Impact Damage to Composites", ASTM STP 568 (ASTM, Philadelphia, 1975) p. 159.
2. N. TAKEDA, R. L. SIERKOWSKI and L. E. MALVERN, *SAMPE Quart.* **12** (1981) 9.
3. L. J. BROUTMAN, "Modern Composite Materials", edited by L. J. Broutman and H. Krock (Addison-Wesley, New York, 1967) Chap. 13.
4. H. T. HAHN and S. W. TSAI, *J. Comp. Mater.* **8** (1974) 288.
5. J. BAX, *Plast. Polymers* **38** (1970) 27.
6. M. L. C. JONES and D. HULL, *J. Mater. Sci.* **14** (1979) 165.
7. K. L. REIFSNIDER, E. G. HENNEKE and W. W. STINCHCOMB, Proceedings of the 4th International Conference on Compositie Materials: Testing and Design, ASTM STP 617 (ASTM, Philadelphia, 1977) p. 93.
8. K. L. REIFSNIDER and A. TALUG, Proceedings of the Research Workshop on Mechanics of Composite Materials, (Duke University, Durham, NC, 1978) p. 130.
9. J. A. KIES, U.S. Naval Research Lab. Report Number 5752 (1962).
10. J. C. SHULTZ, 18th Annual Conference of the SPI Reinforced Plastics Division Sec. 7-D February, 1963.
11. L. R. HERRMANN and K. S. PISTER, ASTM Paper 62-WA-239 (1963).
12. A. PUCK and W. SCHNEIDER, *Plast. Polymers* **37** (1969) 33.
13. K. W. GARRETT and J. E. BAILEY, *J. Mater. Sci.* **12** (1977) 157.
14. G. T. STEVENS and A. W. LUPTON, *ibid* **12** (1977) 1706.
15. Y. C. FUNG, "Foundations of Solid Mechanics" (Prentice-Hall, Inc., Englewood Cliffs, NJ, 1965) p. 463.

Received 15 October
and accepted 14 November 1980

N. TAKEDA*
R. L. SIERAKOWSKI
L. E. MALVERN
Department of Engineering Sciences,
University of Florida,
Gainesville,
Florida 32611,
USA

*Present address: Institute of Space and Aeronautical Science, University of Tokyo, Komaba, Tokyo, Japan.

Electrical conduction in $Na_3H(SO_4)_2$ and $(NH_4)_3H(SO_4)_2$ crystals

Electrical transport in hydrogen-bonded lattices like potassium dihydrogen phosphate (KDP), potassium hydrogen sulphate etc. has been systematically and widely studied and it has been established beyond doubt that the charge carriers are protons [1–6]. Trisodium hydrogen sulphate is a hydrogen-bonded system. Infrared absorption studies [7] as well as X-ray crystal structure determination [8] have shown the presence of a HSO_4^- group in trisodium hydrogen sulphate. Electrical conductivity and dielectric loss measurements have been undertaken on $Na_3H(SO_4)_2$ crystals to investigate the mechanism of electrical transport in the lattice. The studies have been extended to the isostructural $(NH_4)_3H(SO_4)_2$ crystals.

Single crystals were grown by slow evaporation of saturated aqueous solutions of $Na_3H(SO_4)_2$ and $(NH_4)_3H(SO_4)_2$. $Na_3H(SO_4)_2$ crystals doped with iron were grown by adding a few drops of ferric sulphate solution to the original solution. The composition of $Na_3H(SO_4)_2$ was checked by comparing the Debye–Scherrer powder diffraction data with ASTM data cards [9, 10]. Electrical conductivity measurements were carried out under 10^{-2} Torr vacuum using a GR 1230 d.c. electrometer/Keithley 610C solid state electrometer. The dielectric loss measurements were carried out on a GR 1620 AP capacitance measuring bridge assembly in the temperature range 60 to 130° C and in

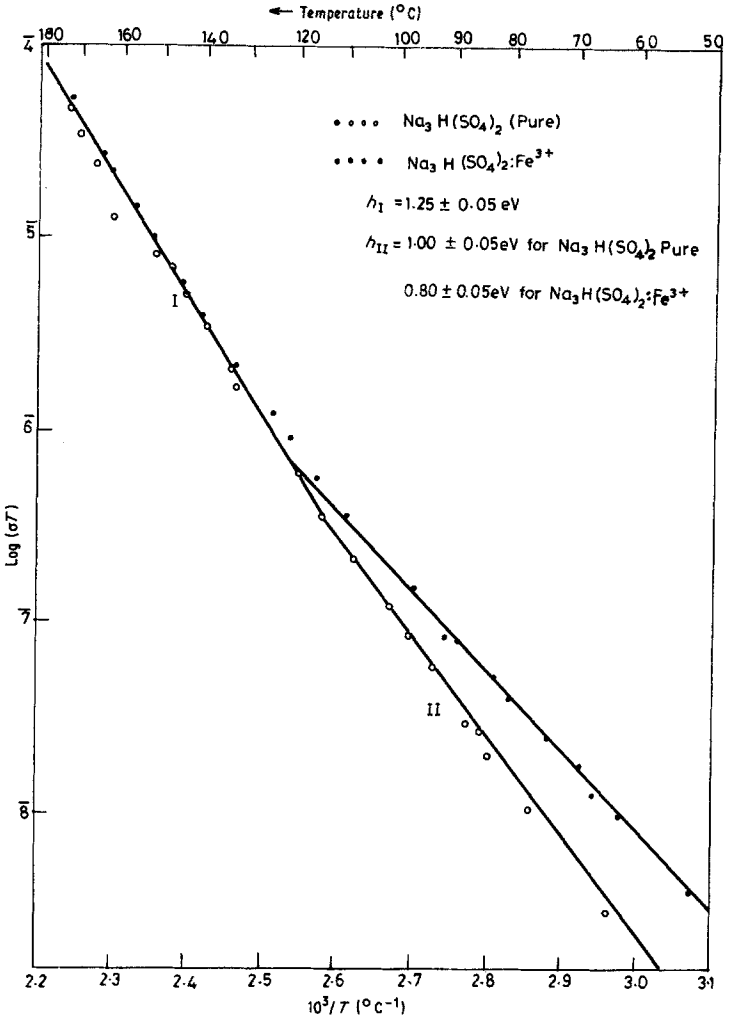

Figure 1 Electrical conductivity of $Na_3H(SO_4)_2$ crystals.

the frequency range 160 to 20 kHz for $Na_3H(SO_4)_2$ crystals. As the conductivity of $(NH_4)_3H(SO_4)_2$ crystals is high, dielectric measurements could not be made on them.

The electrical conductivity data plotted as log (σT) against $(1000/T)$ for $Na_3H(SO_4)_2$ crystals are presented in Fig. 1. The intrinsic regions of both undoped and iron-doped $Na_3H(SO_4)_2$ crystals merge above 120° C and in the structure-sensitive region, the iron-doped crystals show enhanced conductivity with a simultaneous reduction in the activation energy for conduction of 0.80 ± 0.05 eV from a value of 1.00 ± 0.05 eV for undoped crystals. This activation energy of 0.80 eV is too large to compare with 0.49 eV reported for protonic migration in the $KHSO_4$ lattice [5, 6]. The migration energy of cationic vacancies in alkali halide lattices is in the region 0.59 to 0.85 eV [10]. The activation energy for migration of potassium ion vacancies in the K_2SO_4 lattice is reported to be 0.85 eV [12] and is close to the present value. Hence, the electrical conduction in $Na_3H(SO_4)_2$ crystals is more likely to be due to the migration of cationic vacancies rather than interbond protonic jumps.

The starting material (BDH, Analar $NaHSO_4$) is reported to contain about 50 ppm calcium and magnesium, 2 ppm lead and about 4 ppm iron. Calcium, magnesium and lead enter the lattice in their divalent states. Iron seems to exist in its divalent state initially but on irradiation, becomes partially converted to the Fe^{3+} state as seen from the electron spin resonance (ESR) spectra. The doped crystals show ESR of Fe^{3+} ions even before irradi-

TABLE I Electrical conductivity data

Sample	h_1 (eV)	$(\log \sigma T)_{01}$	h_2 (eV)	$(\log \sigma T)_{02}$	h_3 (eV)	$(\log \sigma T)_{03}$	Reference
KDP	–	–	0.99	6.75 (4.25)	0.53	0.77 (−1.73)	[2]
$KHSO_4$	1.21	10.80 (8.30)	–	–	0.49	−2.70 (−5.20)	[5]
$(NH_4)_2SO_4$	–	–	0.76	3.96 (1.46)	–	–	[15]
$Na_3H(SO_4)_2$							
Sample 1	1.25 ± 0.05	10.04	1.00 ± 0.05	7.19	–	–	Present work
Sample 2	1.25 ± 0.05	9.67	1.00 ± 0.05	7.24	–	–	
$Na_3H(SO_4)_2:Fe^{3+}$							
Sample 1	1.25 ± 0.05	10.11	0.80 ± 0.05	4.02	–	–	
Sample 2	1.25 ± 0.05	9.08	0.80 ± 0.05	4.05	–	–	
$(NH_4)_3H(SO_4)_2$	1.00 ± 0.05	10.15	0.70 ± 0.05	6.68	–	–	

Note: Although it is theoretically correct to fit the data to the equation $\sigma = A/T \exp(-h/kT)$, it is conceptual to fit the data to the equation $\sigma = \sigma_0 \exp(-h/kT)$. Hence $\log \sigma_0$ reported by various workers (given in brackets) are corrected to $(\log \sigma T)_0$ by adding $\log T$ where T is an average temperature in the range of measurements expressed in Kelvin.

ation and the intensity of the ESR signal of Fe^{3+} ions is enhanced on irradiation. Thus, in case of undoped crystals, the trace impurity ions are in their divalent state and in the doped ones, iron seems to be present in a state of equilibrium between Fe^{2+} and Fe^{3+}.

The divalent cationic impurities present in the undoped crystals replace the sodium ions and give rise to cationic vacancies. The activation energy of 1.00 eV in the structure-sensitive region could be due to migration of cationic vacancies with a slight degree of association. In the iron-doped crystals, Fe^{3+} replacing the sodium ion could give rise to two cationic vacancies. One of them being in the next nearest neighbour site could be loosely bound to the impurity ion and hence the activation energy of 0.80 eV may be an upper limit for the migration energy of cationic vacancies. Combining this with the activation energy for conduction in the intrinsic region of 1.25 eV, the lower limit for the formation of intrinsic defects will be about 0.90 eV.

Activation energies in the intrinsic regions of $Na_3H(SO_4)_2$ and $KHSO_4$ are nearly equal and the pre-exponential factors are of the same order of magnitude. The complete data of activation energies and the pre-exponential factors for various lattices together with the present data are presented in Table I. From a comparison of the activation energies for $Na_3H(SO_4)_2$ and $KHSO_4$ it would seem that the mechanisms for conduction in the two compounds in the intrinsic regions are similar. Isotope diffusion, deuteration and electrical conductivity measurements have established that the protons are the charge carriers in the extrinsic region of the $KHSO_4$ lattice [5, 6]. This conduction is supposed to be due to the migration of protons along the $H\text{–}SO_4^{2-} \ldots H$ chain-like structure extending in the direction of the a-axis through interbond jumps. There is yet another type of arrangement, in which $(HSO_4^-)_2$ forms a double bridge and is not supposed to contribute to electrical conduction. Absence of protonic conduction in the $Na_3H(SO_4)_2$ lattice could also be due to a closed bridge-type arrangement of protonic bond between two sulphate groups. The large shift in the $\nu_1(HSO_4^-)$ infrared vibration frequency from 885 cm^{-1} [13] to 910 cm^{-1} [7] indicates strong bonding between the proton and the sulphate group. Recent crystal structure determination [8] has shown that two sulphate groups are connected through a single hydrogen bond, thereby forming a closed structure and an O–H ... O bond of length 2.435 Å which is one of the shortest known hydrogen bonds. Hence, protonic conduction through interbond jumps is ruled out.

Crystals heated to above 170° C show cracks and the measurements could not be reproduced if heated above 170° C. Hence, the measurements could not be carried out above 170° C.

$(NH_4)_3H(SO_4)_2$ crystals show two distinct regions of electrical conduction with activation

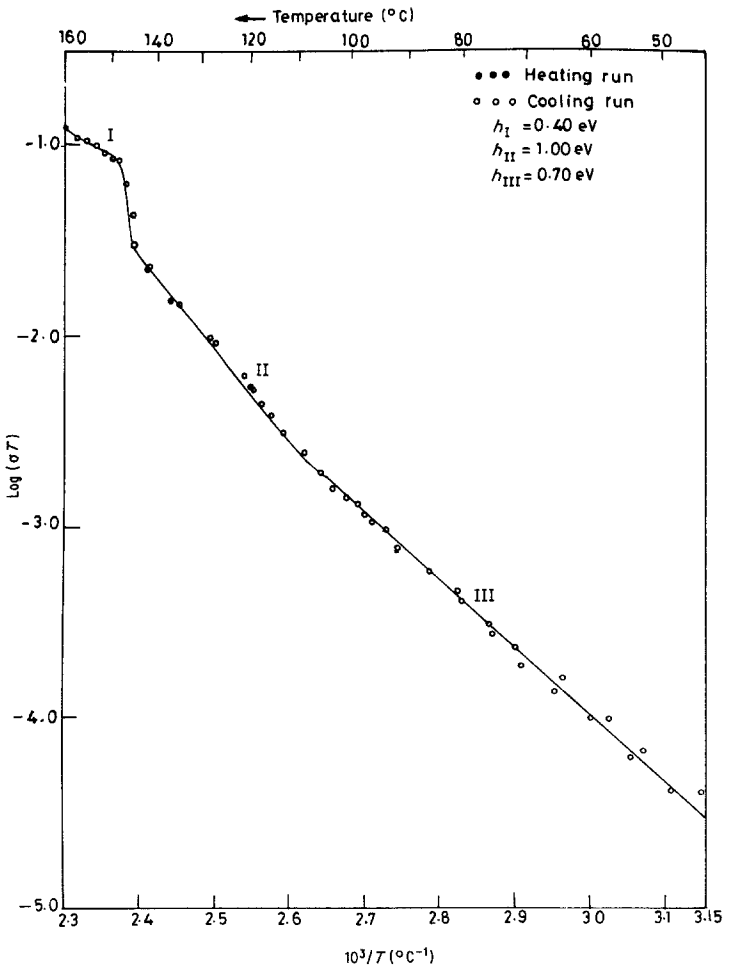

Figure 2 Electrical conductivity of $(NH_4)_3H(SO_4)_2$ crystals. There is a sudden change in the electrical conductivity at the phase transition temperature of 140° C.

energies of 0.70 eV (region III) and 1.00 eV (region II) in the structure-sensitive region and intrinsic regions, respectively, in their conductivity plots (Fig. 2). While passing through a transition from the monoclinic to the trigonal phase at 140° C [14] there is an abrupt change in conductivity. There is no hystersis at the phase transition. In the trigonal phase above 140° C an activation energy of 0.40 eV for conduction is observed. Above 160° C measuresments are not possible as the crystals develop cracks.

The order of magnitude of conductivity is quite high in the extrinsic region compared to that of $(NH_4)_2SO_4$ [15] as may be seen from the pre-exponential factors (Table I). This is possibily due to the migration of NH_4^+ ion vacancies generated due to the presence of divalent background impurities. The activation energy of 0.70 eV is close to that of migration energy of cation vacancies. Recent crystal structure determination [16] shows hydrogen bonding similar to $Na_3H(SO_4)_2$ with a O–H . . . O distance of 2.540 Å. Hence, the protonic conduction seems to be absent in this lattice too. The intrinsic region above 110° C with an activation energy for conduction of 1.00 eV has a pre-exponential factor with the same order of magnitude as for $Na_3H(SO_4)_2$ crystals. It is premature at this stage to draw any conclusions in the absence of tracer diffusion and deuteration data.

Isothermal plots are drawn with tan δ as a function of frequency on a log–log scale in the temperature range 74 to 130° C in Fig. 3. The slopes of these lines are not equal to −1 and approach −1 as the temperature is increased. This may be due to the presence of covalency in the lattice, which

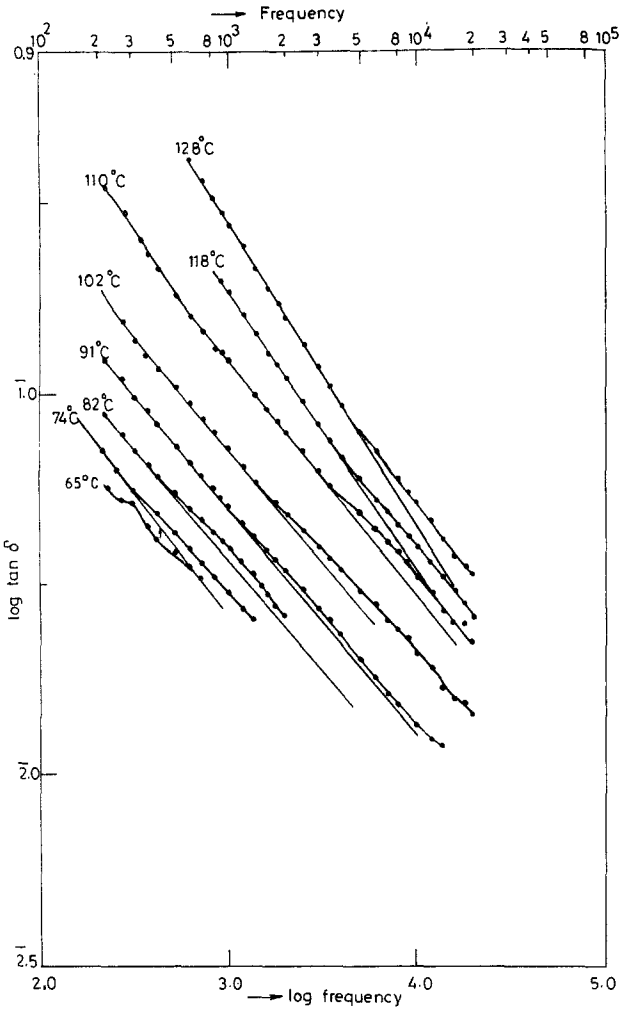

Figure 3 Dielectric loss of $Na_3H(SO_4)_2$ crystals. The log tan–log frequency plots may be seen as straight lines with the departures from the straight lines slowly moving towards the high frequency side with an increase in temperature.

is constraining the motion of ions or dipoles responsible for the dielectric loss. As the temperature is increased, the ions can be expected to be more free and hence, the slope approaches -1.

A kink, possibly due to the presence of dipoles, can be seen at 65° C. As the temperature is increased, the presence of dipolar contribution to the loss can be seen as departures from the straight-line plots, though not significant and the positions of the dielectric peaks could not be ascertained.

References

1. L. GLASER, *Chem. Rev.* **75** (1975) 26.
2. M. O'KEEFFE and C. T. PERRINO, *J. Phys. Chem. Sol.* **28** (1967) 211.
3. *Idem, ibid.* **28** (1967) 1086.
4. L. B. HARRIS and G. J. VELLA, *J. Chem. Phys.* **58** (1973) 4550.
5. M. SHARON and A. K. KALIA, *J. Sol. Stat. Chem.* **38** (1977) 783.
6. C. S. SUNANDANA, *J. Mater. Sci.* **14** (1979) 757.
7. C. RAMASASTRY and K. SUBBA RAMAIAH, unpublished work, 1980.
8. M. CATTI, G. FERRARIS and GABRIELLA, *Acta Cryst.* **B35** (1979) 525.
9. American Society for Testing Metals Data Card No. 2-0294.
10. K. SUBBA RAMAIAH, G. SREENIVASAMURTHY and C. RAMASASTRY, *Z. Kristall.* **147** (1978) 156.
11. P. SUPTITZ and J. TELTOW, *Phys. Stat. Sol.* **23** (1967) 9.
12. B. S. V. S. R. ACHARYULU, Ph. D. thesis, I.I.T., Madras (1972).
13. G. E. WALRAFEN, *J. Chem. Phys.* **39** (1963) 1419.

14. K. GESI, *Phys. Stat. Sol. (a)* **33** (1976) 479.
15. V. H. SCHMIDT, *J. Chem. Phys.* **38** (1963) 2783.
16. S. SUZUKI and V. MAKITA, *Acta Cryst.* **B34** (1978) 732.

Received 15 October
and accepted 14 November 1980

C. RAMASASTRY
K. SUBBA RAMAIAH
Department of Physics,
Indian Institute of Technology,
Madras 600 036,
India

Analysis of thickness distribution and the crystal structure in a Wehner spot

The first observations of anisotropic distribution of sputtered material were reported by Wehner [1] during his investigation of the effects of controlled single crystal sputtering by low energy Hg^+ ions. The same effect was later observed by other authors with different ion–atom pairs at different energies [2, 3]. Silsbee [4] explained this effect by the fact that in the crystal lattice the impulse is better transferred in the close-packed direction of the crystal. Focussing collision sequence efficiently transferred in the close-packed direction is responsible for anisotropic distribution of the material obtained on the collector during sputtering. On further investigation, by photometry of the collector with the sputtered material, it has been found that the material distribution in the spot is subcosinusoidal, which is indicative of higher deposition in the central part of the spot decreasing towards the periphery.

In the present paper the sputtering of Cu monocrystal by Ar^+ ions has been investigated and the distribution of the material in the obtained spots and structural characteristics in their particular zones have been determined. For this investigation the spots lying in the ⟨1 1 0⟩ direction obtained by sputtering the (1 0 0) plane of the monocrystal have been used.

An electromagnetic isotope separation with well defined ion beam energy and incidence angle was used for ion bombardment. Copper monocrystals were sputtered by Ar^+ ions at 10 to 30 keV energy. An ion current density up to 1 mA cm^{-2} and an interaction chamber pressure during bombardment of 6 to 8×10^{-6} Torr was used. The beam diameter was 4 mm and the distance between the target and the collector was about 40 mm. Prior to bombardment, the targets were polished in orthophosphoric acid. The Cu monocrystals were positioned on a separator collector so that the incident ion beam was normal to the (1 0 0) plane of the crystal.

Sputtered material was deposited on to a sphere or a plane glass collector. The sphere collector was used only for the investigation of the anisotropic distribution of the material sputtered from the monocrystal target. To determine the distribution of the material in the spot, the material was deposited onto a plane glass collector which enabled measurement of the spot profile (using a Talystep* profilometer) and sample (thin film) separation from the substrate for electron microscopic investigation. Fig. 1 shows a schematic diagram of the collector arrangement (Fig. 1a) and the zones in the Wehner spot (Fig. 1b).

In order to obtain well separated zones in the spot, many different attempts were made. The best results, which actually made the investigation of the crystal structure possible in particular zones of the spot, were obtained by winding radially 6 to 8 coils of 0.5 mm copper wire at 5 places on the collector plate (Fig. 1b). Thus on the collector, during the bombardment of (1 0 0) planes, several zones were usually obtained with minimum one spot, the structure and thickness of which could be investigated.

The investigation of the spot profile has shown the thickness distribution of the deposited material to be inhomogeneous. The cross-section of the spot was elliptical in form, with the axis $a = 12$ mm and $b = 10$ mm. The thicknesses were measured in the direction of the longer axis at a distance of 3 and 5 mm from the centre. The thickness is highest in the central part of the spot and decreases towards the periphery. The Wehner spot in the ⟨1 1 0⟩ direction, obtained by bombarding a Cu

*Trademark of Johnson Matthey Ltd.

0022–2461/81/072016–04$02.40/0